Characterizing classical periodic orbits from quantum Green's functions in two-dimensional integrable systems: Harmonic oscillators and quantum billiards

Y. F. Chen,[1,*] J. C. Tung,[1] P. H. Tuan,[1] Y. T. Yu,[1] H. C. Liang,[2] and K. F. Huang[1]

[1]*Department of Electrophysics, National Chiao Tung University, 1001 Ta-Hsueh Rd., Hsinchu 30010, Taiwan*

[2]*Institute of Optoelectronic Science, National Taiwan Ocean University, 2 Pei-Ning Rd., Keelung 20224, Taiwan*

(Received 8 September 2016; revised manuscript received 30 December 2016; published 30 January 2017)

A general method is developed to characterize the family of classical periodic orbits from the quantum Green's function for the two-dimensional (2D) integrable systems. A decomposing formula related to the beta function is derived to link the quantum Green's function with the individual classical periodic orbits. The practicality of the developed formula is demonstrated by numerically analyzing the 2D commensurate harmonic oscillators and integrable quantum billiards. Numerical analyses reveal that the emergence of the classical features in quantum Green's functions principally comes from the superposition of the degenerate states for 2D harmonic oscillators. On the other hand, the damping factor in quantum Green's functions plays a critical role to display the classical features in mesoscopic regime for integrable quantum billiards, where the physical function of the damping factor is to lead to the coherent superposition of the nearly degenerate eigenstates.

DOI: 10.1103/PhysRevE.95.012217

I. INTRODUCTION

The Green's function method [1] is widely used in all fields of wave phenomena including acoustics, electrodynamics, and quantum mechanics. Due to the fundamental role in the formulation of quantum theory [2], the quantum Green's function is ubiquitous in various research areas, such as atomic spectroscopy [3], molecular conduction [4], chemical reaction dynamics [5], solid-state physics [6], and much more. The semiclassical formula for quantum Green's function was originally derived by Van Vleck in 1928 [7] and was modified by Gutzwiller in 1967 [8]. Gutzwiller's formula verifies that only the periodic closed orbits from the sum over classical trajectories have essential contributions, whereas the involvements from all other trajectories tend to cancel by destructive interference. Strutinsky *et al.* [9] generalized Gutzwiller's result for the systems with arbitrary symmetries and correspondingly degenerate periodic orbits. Even though the semiclassical formula indicates that the quantum Green's function has an intimate connection with the classical periodic-orbit bundle [10,11], this connection has never been manifested in the spatial distribution of the quantum Green's function so far.

The study of quantum stationary states, in particular, their spatial dependence on the classical dynamics, still has attracted great attention since the advent of quantum mechanics 100 years ago [12–21]. Quantum wave functions correlated with classical periodic orbits have been verified to play an important role in explaining the quantum phenomena such as shell effects in nuclei and metallic clusters [22,23], conductance fluctuations in mesoscopic quantum transports [24,25], and oscillations in photodetachment cross sections [26,27]. On the other hand, thanks to Hamilton's ingenious optico-mechanical theory [28–30], modern laser resonators have been widely exploited to analogously explore the formation of quantum coherent waves in the mesoscopic regime [31–40]. As shown in Fig. 1(a), the wave patterns corresponding to the Lissajous periodic orbits of two-dimensional (2D) commensurate harmonic oscillators have been confirmed to be the predominant modes in the selectively pumped large-Fresnel-number spherical cavity with astigmatism [31–35]. Furthermore, as shown in Fig. 1(b), the lasing modes related to the classical trajectories of quantum square billiards are generally observed in the large-aperture vertical cavity surface emitting lasers (VCSELs) with large detuning [36–40]. Therefore, it will certainly provide important insights into mesoscopic physics as well as laser physics to manifest the connection between the spatial distributions of quantum Green's functions and the classical periodic orbits. More importantly, the harmonic oscillators and quantum billiards are two of the most fundamental systems with applications in diverse fields [18–21,41–43].

In this work, we propose a general method to characterize the family of classical periodic orbits from the energy-dependent Green's functions for the 2D integrable systems. From the wave representation of coherent states in the 2D isotropic harmonic oscillator, we originally develop a decomposition formula related to the beta function to link the quantum Green's function with the individual classical periodic orbits. With the developed formula, the 2D commensurate harmonic oscillators and integrable quantum billiards are numerically analyzed to manifest the connection between the quantum Green's function and the single classical orbits. For the case of the square quantum billiards, it is found that the damping factor plays a critical role to reveal the classical features in the spatial patterns of quantum Green's functions in the mesoscopic regime. The physical role of the damping factor is verified to lead to the coherent superposition of the nearly degenerate eigenstates that generally occurs due to the opening or symmetry-breaking effect. We further verify that the quantum Green's function with an appropriate damping factor can be decomposed to correspond to the individual classical periodic orbit. Since the quantum-classical or ray-wave correspondence has been ubiquitously observed in numerous systems [22–27,31–40], the present analysis can offer important insights into quantum physics, mesoscopic physics, and laser physics.

*Corresponding author: yfchen@cc.nctu.edu.tw

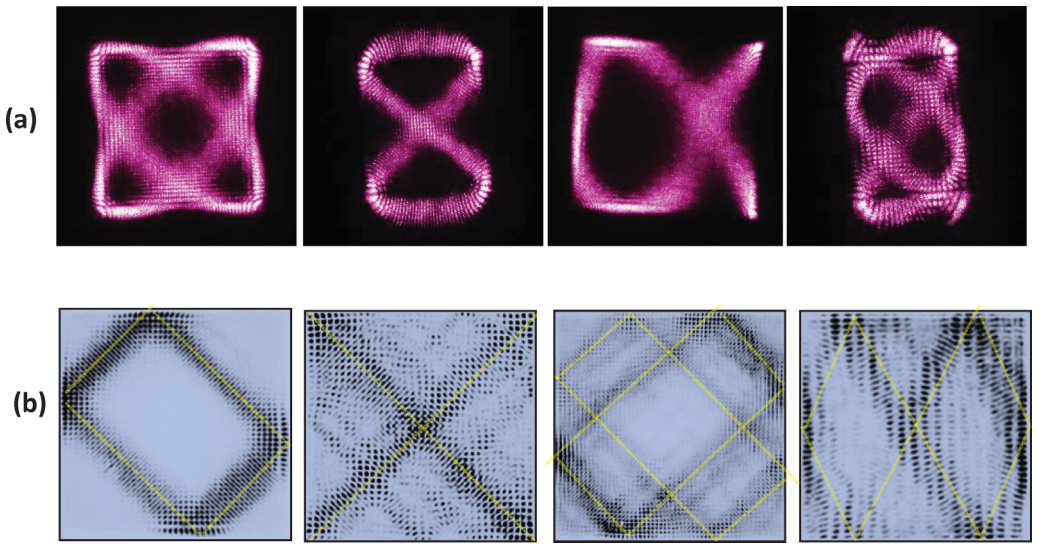

FIG. 1. (a) Lasing modes generally observed in the selectively pumped large-Fresnel-number spherical cavity with astigmatism [31–35]. (b) Lasing modes generally observed in the large-aperture VCSELs with large detuning [36–40].

II. CHARACTERIZING CLASSICAL PERIODIC ORBITS FROM QUANTUM GREEN'S FUNCTIONS IN 2D INTEGRABLE SYSTEMS

The time-dependent propagator that describes the propagation of a particle from $\mathbf{r}' \to \mathbf{r}$ in a time interval $t - t' > 0$ is given by [11]

$$K(\mathbf{r},\mathbf{r}';t-t') = \sum_n \psi_n^*(\mathbf{r}')\ \psi_n(\mathbf{r})\ e^{-iE_n(t-t')/\hbar}, \qquad (1)$$

where the normalized eigenstates $\{\psi_n(\mathbf{r})\}$ satisfy the equation $\hat{H}\psi_n(\mathbf{r}) = E_n\,\psi_n(\mathbf{r})$ and E_n are the eigenvalues of the Hamiltonian $\hat{H}$. In terms of the Fourier transform of the time-dependent propagator $K(\mathbf{r},\mathbf{r}';t-t')$, the quantum Green's function in energy representation is defined as [11]

$$G(\mathbf{r},\mathbf{r}';E) = -\frac{i}{\hbar}\lim_{\Gamma\to 0}\int_0^\infty K(\mathbf{r},\mathbf{r}';t)\ e^{i(E+i\gamma)t/\hbar}dt$$
$$= \lim_{\Gamma\to 0}\sum_n \frac{\psi_n^*(\mathbf{r}')\ \psi_n(\mathbf{r})}{E+i\gamma-E_n}\,. \qquad (2)$$

It can be shown that the Green's function $G(\mathbf{r},\mathbf{r}';E)$ satisfies the equation

$$(\hat{H}-E)\,G(\mathbf{r},\mathbf{r}';E) = -\delta(\mathbf{r}-\mathbf{r}'). \qquad (3)$$

The singularity structure of Green's functions reflects the spectrum of the energy levels.

Considering the 2D integrable systems with quantum numbers (n_1,n_2) and eigenvalues E_{n_1,n_2}, the quantum Green's function can be given by

$$G(\mathbf{r},\mathbf{r}';E) = \lim_{\gamma\to 0}\sum_{n_2=0}\sum_{n_1=0}\frac{\psi_{n_1,n_2}^*(x',y')\ \psi_{n_1,n_2}(x,y)}{E+i\gamma-E_{n_1,n_2}}\,. \qquad (4)$$

Since the quantum Green's function contains all classical periodic-orbit bundles, it is an interesting issue how to characterize single classical trajectories from $G(\mathbf{r},\mathbf{r}';E)$. In classical mechanics, the initial conditions for specifying the individual classical trajectory includes not only the initial position (x',y') but also the energy fractions in the x and y directions. It has been verified that the coherent states of the 2D harmonic oscillator exactly correspond to the single periodic orbits [16]. Here the representation of the coherent state is exploited to derive the mathematical form for the energy fractions in the x and y directions for characterizing the family of classical orbits from $G(\mathbf{r},\mathbf{r}';E)$.

The time-dependent coherent state for the 2D isotropic quantum harmonic oscillator is given by [16]

$$\Psi_{cs}(x,y,t) = \sum_{n_2=0}\sum_{n_1=0}\frac{(\bar{n}_1)^{n_1/2}}{\sqrt{n_1!}}\frac{(\bar{n}_2)^{n_2/2}}{\sqrt{n_2!}}$$
$$\times\, e^{-(\bar{n}_1+\bar{n}_2)/2}\psi_{n_1,n_2}(x,y)\,e^{-i(n_1+n_2+1)(\omega_0 t-\varphi)}, \qquad (5)$$

where $\bar{n}_1$ and $\bar{n}_2$ are the mean orders in the x and y directions, respectively. Using the constant energy to rearrange the summation in Eq. (5), the time-dependent coherent state can be rewritten as

$$\Psi_{cs}(x,y,t) = \sum_{N=0}\frac{(\bar{N})^{N/2}}{\sqrt{(N+1)!}}\,e^{-\bar{N}/2}$$
$$\times\, e^{-i(N+1)(\omega_0 t-\varphi)}\ \Psi_N(x,y,u), \qquad (6)$$

where $\bar{N} = \bar{n}_1 + \bar{n}_2$, $u = \bar{n}_1/\bar{N}$, and the stationary coherent state $\Psi_N(x,y,u)$ is given by

$$\Psi_N(x,y,u) = \sum_{n_1+n_2=N} C_{n_1,n_2}(u)\ \psi_{n_1,n_2}(x,y)\,, \qquad (7)$$

where

$$C_{n_1,n_2}(u) = \frac{\sqrt{(n_1+n_2+1)!}}{\sqrt{n_1!n_2!}}(u)^{n_1/2}(1-u)^{n_2/2}. \qquad (8)$$

The intensity $|\Psi_N(x,y,u)|$ of the stationary coherent state $\Psi_N(x,y,u)$ has been shown to correspond to the classical periodic orbit precisely [16]. The weighting coefficients $C_{n_1,n_2}(u)$ in Eq. (8) for the coherent state $\Psi_N(x,y,u)$ can be

related to the beta function that is defined as [44]

$$B(n,m) = \int_0^1 u^{n-1}(1-u)^{m-1}\, du = \frac{\Gamma(n)\,\Gamma(m)}{\Gamma(n+m)}, \quad (9)$$

where $\Gamma(\cdot)$ is the gamma function. The beta function in Eq. (9) can be used to verify that the weighting coefficients $C_{n_1,n_2}(u)$ satisfy the normalization

$$\int_0^1 [C_{n_1,n_2}(u)]^2\, du = 1. \quad (10)$$

Since the stationary coherent state $\Psi_N(x,y,u)$ exactly corresponds to the single periodic orbit, we propose to exploit the probability $[C_{n_1,n_2}(u)]^2$ to decompose the quantum Green's function $G(\mathbf{r},\mathbf{r}';E)$. By inserting the probability $[C_{n_1,n_2}(u)]^2$ into the summation of Eq. (4), the quantum Green's function can be decomposed as

$$g(\mathbf{r},\mathbf{r}';E,u) = \lim_{\gamma\to 0}\sum_{n_2=0}\sum_{n_1=0}[C_{n_1,n_2}(u)]^2 \times \frac{\psi^*_{n_1,n_2}(x',y')\,\psi_{n_1,n_2}(x,y)}{E+i\gamma-E_{n_1,n_2}}. \quad (11)$$

Using Eqs. (10) and (11), it can be found that $G(\mathbf{r},\mathbf{r}';E)$ and $g(\mathbf{r},\mathbf{r}';E,u)$ satisfy

$$G(\mathbf{r},\mathbf{r}';E) = \int_0^1 g(\mathbf{r},\mathbf{r}',E,u)\, du. \quad (12)$$

As demonstrated in the following section, the present approach can be used as a general procedure for other 2D integrable systems, as long as the relationship between the parameter u and the classical periodic orbits is determined. Nevertheless, it is worthwhile to mention that the present method is not effective for extracting the wave functions with scars, which are associated with the unstable periodic orbits in the chaotic billiards. Even though the wave functions with scars are very special to be related to the unstable periodic orbits, they are the eigenfunctions in the systems. Since the eigenvalues of the chaotic billiards are significantly repelled, the Green's functions in Eq. (2) are generally contributed by one and only one eigenfunction. Consequently, the wave functions with scars can be directly obtained with the Green's functions. More specifically, the Green's functions in the integrable systems are generally associated with an ensemble of classical periodic orbits, whereas in the chaotic billiards the eigenfunctions related to the single unstable periodic orbits can be directly obtained from the Green's functions without any decomposition procedure.

III. DECOMPOSING QUANTUM GREEN'S FUNCTIONS IN 2D COMMENSURATE HARMONIC OSCILLATORS

Considering the 2D commensurate harmonic oscillator, the Hamiltonian operator $\hat{H}$ is given by

$$\hat{H} = -\frac{\hbar^2}{2m}\left(\frac{d^2}{dx^2}+\frac{d^2}{dy^2}\right)+\frac{1}{2}m\left(\omega_1^2x^2+\omega_2^2y^2\right), \quad (13)$$

where m is the oscillator mass, and ω_1 and ω_2 are the natural frequencies in the x and y directions, respectively. For convenience, we set $\omega_1 = q\omega_0$ and $\omega_2 = p\omega_0$, where p and q are coprime integers, and ω_0 is the common factor of the frequencies. In terms of the dimensionless parameters $\tilde{x} = x\sqrt{qm\omega_0/\hbar}$ and $\tilde{y} = y\sqrt{pm\omega_0/\hbar}$, the Hamiltonian operator in Eq. (13) can be rewritten as

$$\hat{H} = \hbar\omega_0\left[\frac{1}{2}q\left(-\frac{d^2}{d\tilde{x}^2}+\tilde{x}^2\right)+\frac{1}{2}p\left(-\frac{d^2}{d\tilde{y}^2}+\tilde{y}^2\right)\right]. \quad (14)$$

The eigenfunctions and eigenvalues for Eq. (14) can be given by [2]

$$\psi_{n_1,n_2}(\tilde{x},\tilde{y}) = \left(2^{n_1+n_2-1}n_1!\,n_2!\,\pi\right)^{-1/2} \times e^{-(\tilde{x}^2+\tilde{y}^2)/2}H_{n_1}(\tilde{x})H_{n_2}(\tilde{y}), \quad (15)$$

$$E_{n_1,n_2} = \hbar\omega_0\left[q(n_1+1/2)+p(n_2+1/2)\right]. \quad (16)$$

Here $H_n(\cdot)$ is the Hermite polynomials of order n. Substituting Eqs. (15) and (16) into Eq. (4), the quantum Green's function is given by

$$G(\tilde{\mathbf{r}},\tilde{\mathbf{r}}';E) = \lim_{\gamma\to 0}\sum_{n_2=0}\sum_{n_1=0}\frac{\psi^*_{n_1,n_2}(\tilde{x}',\tilde{y}')\,\psi_{n_1,n_2}(\tilde{x},\tilde{y})}{E+i\gamma-E_{n_1,n_2}}, \quad (17)$$

where $\tilde{\mathbf{r}}' = (\tilde{x}',\tilde{y}')$, $\tilde{\mathbf{r}} = (\tilde{x},\tilde{y})$, $\tilde{x}' = x'\sqrt{qm\omega_0/\hbar}$, and $\tilde{y}' = y'\sqrt{pm\omega_0/\hbar}$. Using p and q as the divisors, the indices n_1 and n_2 can be expressed as $n_1 = pk_1+\lambda_1$ and $n_2 = qk_2+\lambda_2$, where k_1 and k_2 are the quotients and λ_1 and λ_2 are the remainders. Consequently, the eigenenergy can be normalized as

$$\varepsilon_{N,\lambda_1,\lambda_2} = E_{n_1,n_2}/\hbar\omega_0 = Nqp+q(\lambda_1+1/2)+p(\lambda_2+1/2), \quad (18)$$

where $N = k_1+k_2$. For the resonant condition, $E = E_{n_1,n_2}$, the quantum Green's function in Eq. (17) can be expressed as a superposition of the degenerate eigenstates satisfying $N = k_1+k_2$. Since the remainders (λ_1,λ_2) essentially do not affect the spatial characteristics of the quantum Green's function $G(\tilde{\mathbf{r}},\tilde{\mathbf{r}}';E)$, the condition of $\lambda_1 = \lambda_2 = 0$ is used in the following analysis unless otherwise specified.

The connection between quantum Green's functions and classical periodic orbits can be manifested by plotting the bundle structure of classical trajectories starting from the initial position $(\tilde{x}',\tilde{y}')$ at constant energy ε. The classical periodic orbits can be found by using $\tilde{x}(t) = \sqrt{2n_1+1}\sin(q\omega_0t+\phi_1)$ and $\tilde{y}(t) = \sqrt{2n_2+1}\sin(p\omega_0t+\phi_2)$, where all (n_1,n_2) and (ϕ_1,ϕ_2) are solved from the constraints of $\tilde{x}' = \sqrt{2n_1+1}\sin\phi_1$, $\tilde{y}' = \sqrt{2n_2+1}\sin\phi_2$, and $n_1+n_2 = Nqp$. First of all, we consider the initial position to be just at the center, i.e., $(\tilde{x}',\tilde{y}') = (0,0)$. The first column in Fig. 2 shows the calculated results for the spatial patterns of $|G(\tilde{\mathbf{r}},\tilde{\mathbf{r}}';E)|$ with the energy of $N = 34$ for three cases of $(q,p) = (1,1)$, $(q,p) = (2,1)$, and $(q,p) = (2,3)$. Three different total numbers of classical trajectories 6, 12, and 1000 are plotted in Fig. 2 from the second to fourth columns to reveal the formation of periodic-orbit bundles. In the plot formed by 1000 trajectories, the density of the drawing points is controlled to be 90 points for each periodic orbit to mimic the interference patterns of quantum Green's functions, where each drawing point is located at a constant time interval. As seen in Fig. 2, the spatial distributions of quantum Green's functions can be linked to classical periodic-orbit bundles

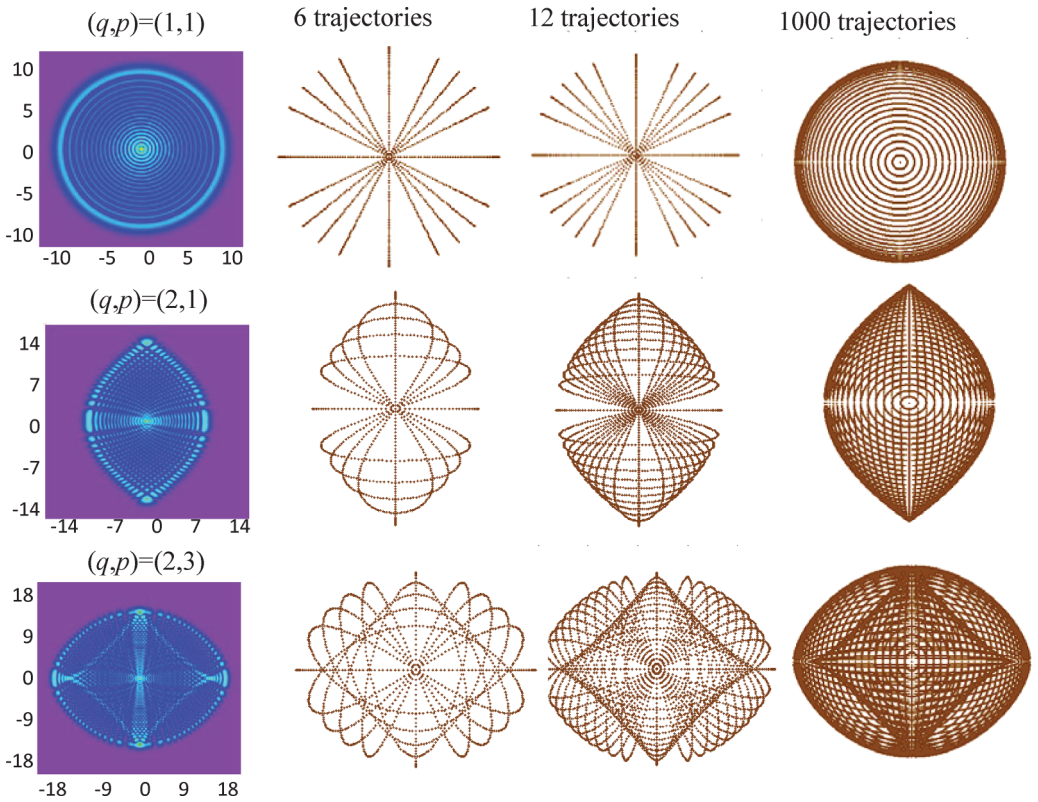

FIG. 2. First column: calculated results for the spatial patterns of $|G(\tilde{\mathbf{r}},\tilde{\mathbf{r}}';E)|$ with the energy of $N = 34$ and $(\tilde{x}',\tilde{y}') = (0,0)$ for three cases of $(q,p) = (1,1)$, $(q,p) = (2,1)$, and $(q,p) = (2,3)$. Second through fourth columns: different total numbers of classical trajectories 6, 12, and 1000 to reveal the formation of periodic-orbit bundles.

for all cases. For $(q,p) = (1,1)$, the classical trajectories are formed by various linear orbits. For $(q,p) = (2,1)$ and $(q,p) = (2,3)$, the classical trajectories are composed of the so-called Lissajous figures with symmetry.

Next, the initial position of $(\tilde{x}',\tilde{y}') = (3,0)$ is numerically analyzed to explore the off-center effect. Figure 3 shows the same plots as in Fig. 2 for the calculated results with $(\tilde{x}',\tilde{y}') = (3,0)$ and $N = 34$. The intensity of the wave pattern $|G(\tilde{\mathbf{r}},\tilde{\mathbf{r}}';E)|$ is essentially distributed on the regions corresponding to the area formed by all classical trajectories passing through the position $(\tilde{x}',\tilde{y}')$. The initial position $(\tilde{x}',\tilde{y}')$ can be seen to be a focal point in the intensity distribution of the wave pattern $|G(\tilde{\mathbf{r}},\tilde{\mathbf{r}}';E)|$, which well corresponds to the classical feature. For $(q,p) = (1,1)$, the classical trajectories comprise various elliptical orbits. For $(q,p) = (2,1)$ and $(q,p) = (2,3)$, the classical trajectories are composed of the asymmetric Lissajous figures. As a result, the symmetry breaking in the spatial patterns of $|G(\tilde{\mathbf{r}},\tilde{\mathbf{r}}';E)|$ caused by the off-center position $(\tilde{x}',\tilde{y}')$ can be clearly manifested.

Figure 4 shows the several calculated results for $|G(\tilde{\mathbf{r}},\tilde{\mathbf{r}}';E)|$ and $|g(\tilde{\mathbf{r}},\tilde{\mathbf{r}}';E,u)|$ with $(\tilde{x}',\tilde{y}') = (3,0)$ and $u = 0, 0.2, 0.5, 0.8$, and 1.0 for $(q,p) = (1,1)$ with $N = 80$, $(q,p) = (2,1)$ with $N = 60$, and $(q,p) = (2,3)$ with $N = 40$. For $(q,p) = (2,1)$ and $(q,p) = (2,3)$, the wave patterns $|g(\tilde{\mathbf{r}},\tilde{\mathbf{r}}';E,u)|$ can be seen to be well localized on the regions corresponding to the single classical periodic orbits. Moreover, the wave intensities illustrate geometrically Bohr's correspondence principle: the velocity of the classical particle is at local minima at the returning points of the motion, and therefore the amplitude has local maxima at these points. For $(q,p) = (1,1)$ with $u \neq 0$, the wave patterns of $|g(\tilde{\mathbf{r}},\tilde{\mathbf{r}}';E,u)|$ reveal two periodic orbits that are degenerate due to the symmetric effect. To be brief, the beta distribution can be used to decompose the Green's function $G(\tilde{\mathbf{r}},\tilde{\mathbf{r}}';E)$ into $g(\tilde{\mathbf{r}},\tilde{\mathbf{r}}';E,u)$ in Eq. (12) to represent the single or degenerate periodic orbits. Next, the functions $G(\tilde{\mathbf{r}},\tilde{\mathbf{r}}';E)$ and $g(\tilde{\mathbf{r}},\tilde{\mathbf{r}}';E,u)$ are further extended to explore the characteristics of quantum Green's functions in 2D integrable billiards.

IV. DECOMPOSING QUANTUM GREEN'S FUNCTIONS IN SQUARE AND CIRCULAR BILLIARDS

For a square billiard in the region of $0 \leqslant x \leqslant a$ and $0 \leqslant y \leqslant a$, the eigenfunctions and eigenvalues are given by

$$\Psi_{n_1,n_2}(x,y) = \frac{2}{a}\,\sin\left(\frac{n_1\pi}{a}x\right)\sin\left(\frac{n_2\pi}{a}y\right), \tag{19}$$

$$E_{n_1,n_2} = \frac{\hbar^2}{2m}k^2_{n_1,n_2} = \frac{\hbar^2}{2m}\left(\frac{\pi}{a}\right)^2\left(n_1^2+n_2^2\right). \tag{20}$$

Since the degenerate eigenstates are occasional and rare, the quantum Green's function in Eq. (2) with $\gamma \to 0$ is generally the superposition of few eigenfunctions with accidental degeneracy. Consequently, the formula in Eq. (2) cannot be directly exploited to make a connection with classical dynamics for the finite energies. Noticeably, it has been experimentally confirmed [36] that the tiny opening or symmetry-breaking effect usually causes the superposition of the nearly degenerate

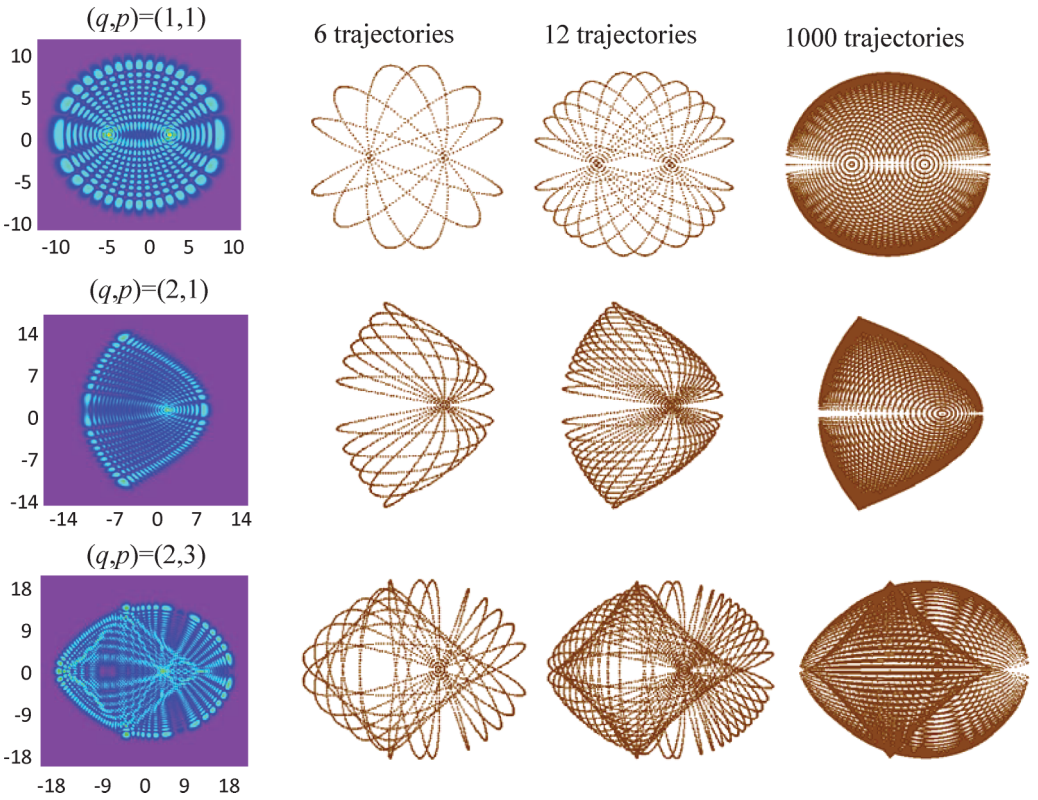

FIG. 3. The same as Fig. 1 for $(\tilde{x}', \tilde{y}') = (3, 0)$.

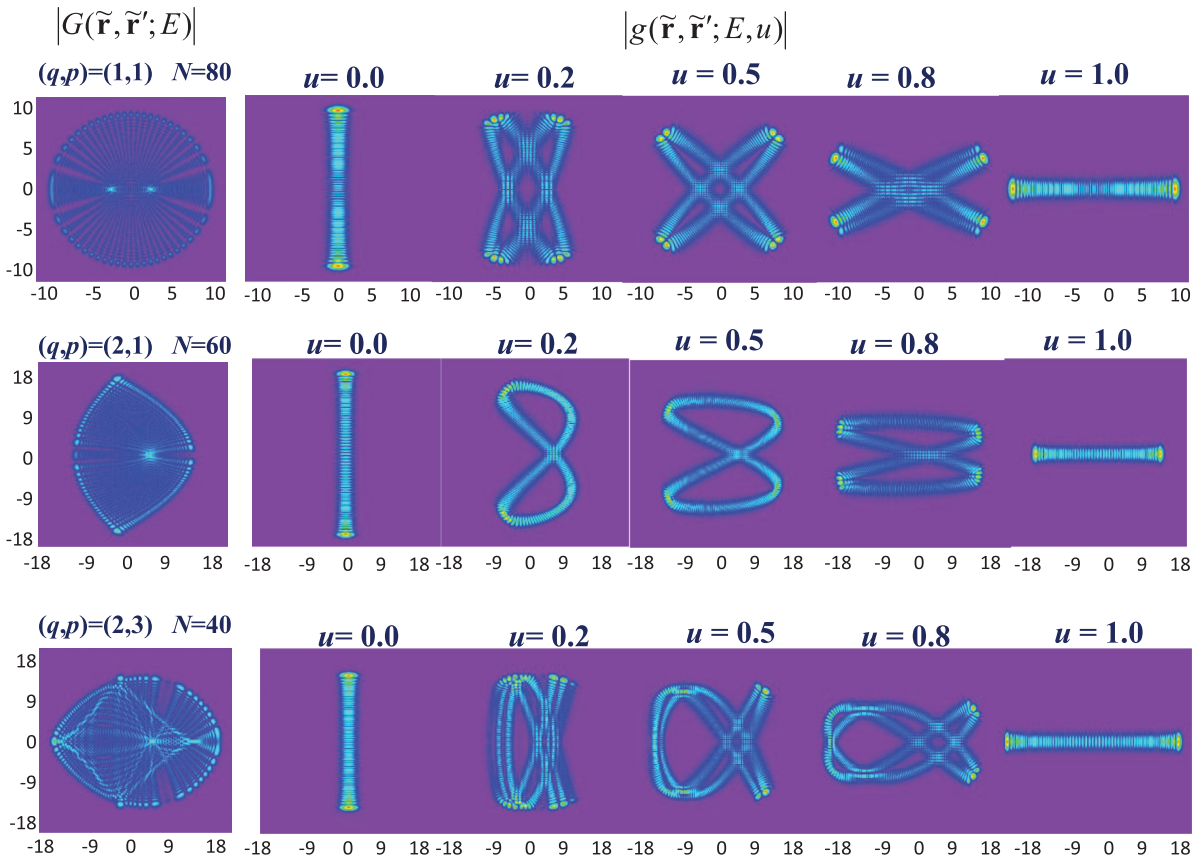

FIG. 4. Several calculated results for $|G(\tilde{\mathbf{r}}, \tilde{\mathbf{r}}'; E)|$ and $|g(\tilde{\mathbf{r}}, \tilde{\mathbf{r}}'; E, u)|$ with $(\tilde{x}', \tilde{y}') = (3, 0)$ and $u = 0, 0.2, 0.5, 0.8$, and 1.0 for $(q, p) = (1, 1)$ with $N = 80$, $(q, p) = (2, 1)$ with $N = 60$, and $(q, p) = (2, 3)$ with $N = 40$.

eigenstates, leading to the emergence of classical features. The superposition of the nearly degenerate eigenstates can be considered by using a nonzero damping coefficient γ. Therefore, it is practically important to consider the damping effect in the quantum Green's function for the integrable systems with rare degeneracies.

In terms of the wave number k with the damping coefficient γ, the quantum Green's functions and the decomposition formula for 2D square billiards can be given by

$$G(\mathbf{r},\mathbf{r}';k,\gamma) = \sum_{n_2=1}\sum_{n_1=1} \frac{\Psi^*_{n_1,n_2}(x',y')\,\Psi_{n_1,n_2}(x,y)}{(k+i\gamma)^2 - k^2_{n_1,n_2}}, \quad (21)$$

$$g(\mathbf{r},\mathbf{r}';k,\gamma,u) = \sum_{n_2=1}\sum_{n_1=1} [C_{n_1,n_2}(u)]^2 \times \frac{\Psi^*_{n_1,n_2}(x',y')\,\Psi_{n_1,n_2}(x,y)}{(k+i\gamma)^2 - k^2_{n_1,n_2}}. \quad (22)$$

The distribution $[C_{n_1,n_2}(u)]^2$ gives the result of $\bar{n}_1/\bar{n}_2 = u/(1-u)$, where $\bar{n}_1$ and $\bar{n}_2$ are the mean values of the quantum numbers n_1 and n_2, respectively. For a 2D square billiard, the energy ratio between the x and y directions is given by $E_x/E_y = (\bar{n}_1/\bar{n}_2)^2$ from quantum mechanics and $E_x/E_y = (v_x/v_y)^2$ from classical mechanics, where v_x/v_y is the velocity ratio between the x and y directions. As a result, the parameter u in Eq. (22) is related to the velocity ratio as $u/(1-u) = v_x/v_y$. The effect of the damping coefficient γ can be manifested from the correspondence between $g(\mathbf{r},\mathbf{r}';k,\gamma,u)$ and periodic orbits. The periodic orbits can be denoted by the indices (P,Q), where P and Q are two coprime integers describing the numbers of collisions with the horizontal and vertical walls in a round-trip. Using the classical dynamics of $v_x/v_y = Q/P$, the relationship between u and (P,Q) can be found to be $u = Q/(P+Q)$. In terms of (P,Q), the path lengths of the periodic orbits are generally given by $L_{P,Q} = 2a\sqrt{P^2+Q^2}$. Thorough computations indicate that the dimensionless parameter ξ defined as $\xi = 2\gamma L_{P,Q}/\pi$ can be used to characterize the critical value of the damping coefficient for manifesting the periodic orbit (P,Q) in $|g(\mathbf{r},\mathbf{r}';k,\gamma,u)|$. Figure 5 shows the numerical patterns of $|G(\mathbf{r},\mathbf{r}';k,\gamma)|$ (upper row) and $|g(\mathbf{r},\mathbf{r}';k,\gamma,u)|$ (lower row) for several damping factors of $\xi = 0.3$, 1.0, 3.0, and 5.0 with the parameters of $(P,Q) = (2,1)$, $u = 1/3$, $(x',y') = (a/2\,,a/2)$, and $k = \pi M/a$ with $M = 24\sqrt{5}$. It can be seen that for $\xi = 1.0$ the wave pattern $|g(\mathbf{r},\mathbf{r}';k,\gamma,u)|$ is well concentrated on the classical periodic orbit. For $\xi = 0.3$, both of the wave patterns $|G(\mathbf{r},\mathbf{r}';k,\gamma)|$ and $|g(\mathbf{r},\mathbf{r}';k,\gamma,u)|$ extensively spread in the billiard region. Numerical results reveal that the overall patterns are almost unchanged for $\xi \leqslant 0.3$. On the other hand, the wave patterns $|G(\mathbf{r},\mathbf{r}';k,\gamma)|$ and $|g(\mathbf{r},\mathbf{r}';k,\gamma,u)|$ can be found to be strongly localized on the initial position $(x',y') = (a/2,a/2)$ for $\xi \geqslant 3.0$, as shown in Figure 5. For $\xi > 1.0$, the larger the damping factor ξ is, the more localized the quantum Green's function will become.

For a fixed k and γ, the quantum Green's function $G(\mathbf{r},\mathbf{r}';k,\gamma)$ can be decomposed into different $g(\mathbf{r},\mathbf{r}';k,\gamma,u)$ to correspond to different periodic orbits by varying the value of u. The first row of Fig. 6 shows the numerical patterns of $|G(\mathbf{r},\mathbf{r}';k,\gamma)|$ and $|g(\mathbf{r},\mathbf{r}';k,\gamma,u)|$ for three different values of u with the parameters of $(x',y') = (a/2,a/2)$, $\gamma = 0.1\pi/a$, and $k = \pi M/a$ with $M = 120$. Note that the values of $u = 1/2$, $1/3$, and $3/5$ in Fig. 6 correspond to the periodic orbits with $(P,Q) = (1,1)$, (2,1), and (2,3), respectively. Moreover, the periodic orbits are dependent not only on (P,Q) but also on (x',y'). The second row of Fig. 6 shows the numerical patterns of $|G(\mathbf{r},\mathbf{r}';k,\gamma)|$ and $|g(\mathbf{r},\mathbf{r}';k,\gamma,u)|$ for the off-center initial position of $(x',y') = (a/2,a/4)$ for three different values of u with the parameters of $\gamma = 0.1\pi/a$ and $k = \pi M/a$ with $M = 120$. It is intriguing that even though the patterns of $|G(\mathbf{r},\mathbf{r}';k,\gamma)|$ exhibit the extensive ridge structures, the patterns of $|g(\mathbf{r},\mathbf{r}';k,\gamma,u)|$ are well concentrated on the classical periodic orbits for different u. In other words, decomposing $G(\mathbf{r},\mathbf{r}';k,\gamma)$ into $g(\mathbf{r},\mathbf{r}';k,\gamma,u)$ can clearly manifest the quantum-classical correspondence.

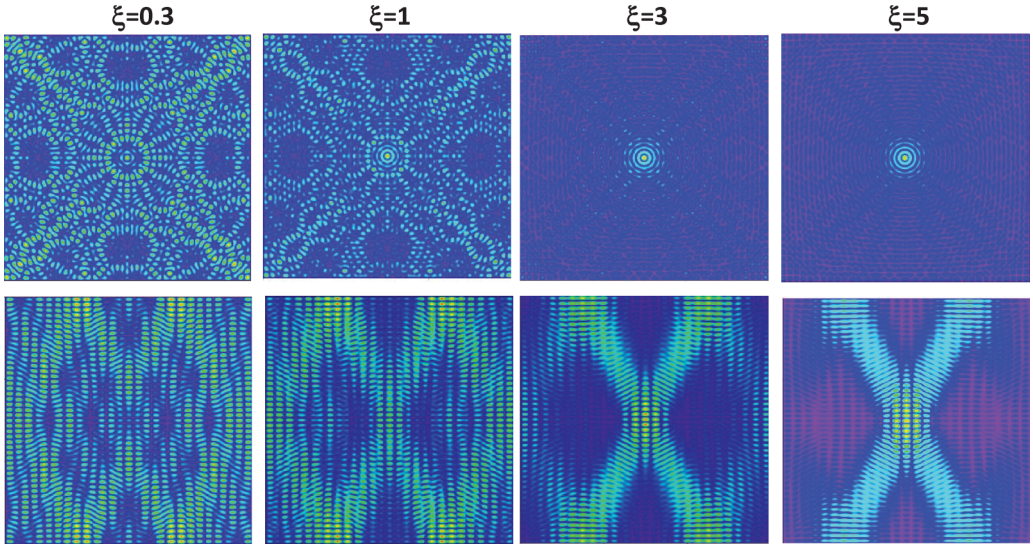

FIG. 5. Numerical patterns of $|G(\mathbf{r},\mathbf{r}';k,\gamma)|$ (upper row) and $|g(\mathbf{r},\mathbf{r}';k,\gamma,u)|$ (lower row) for several damping factors of $\xi = 0.3$, 1.0, 3.0, and 5.0 with parameters of $(P,Q) = (2,1)$, $u = 1/3$, $(x',y') = (a/2\,,a/2)$, and $k = \pi M/a$ with $M = 24\sqrt{5}$.

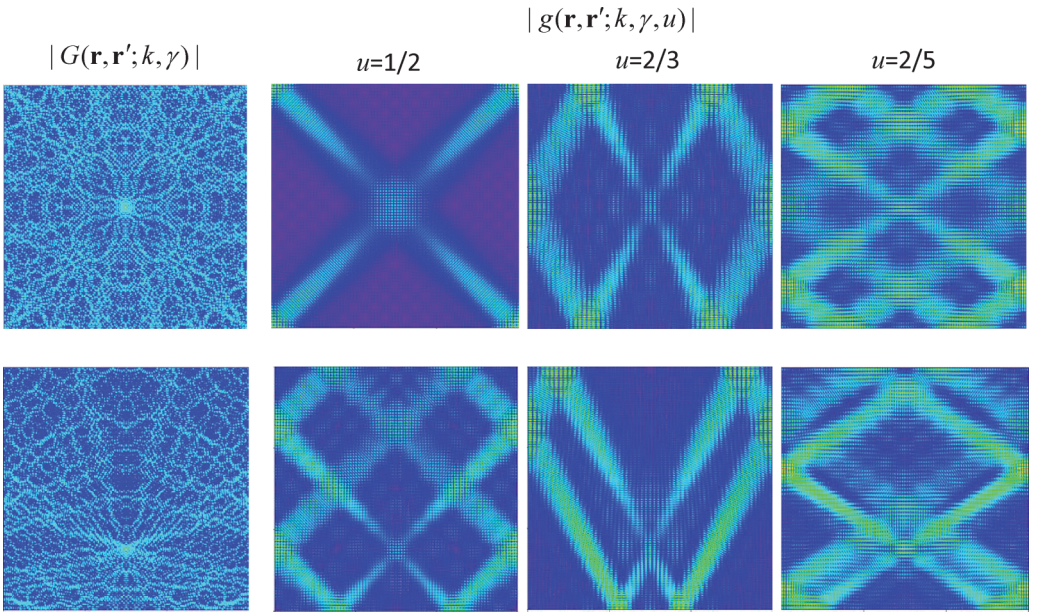

FIG. 6. Numerical patterns of $|G(\mathbf{r},\mathbf{r}';k,\gamma)|$ and $|g(\mathbf{r},\mathbf{r}';k,\gamma,u)|$ for three different values of u with the parameters of $\gamma = 0.1\pi/a$ and $k = \pi M/a$ with $M = 120$. First row: $(x',y') = (a/2, a/2)$; second row: $(x',y') = (a/2, a/4)$.

The present approach can be applied to other 2D integrable systems. For example, the periodic orbits of a circular billiard are characterized by the indices (p,q), where q is the number of turning points at the boundary during one period, and p is the number of windings during one period. By using the Wentzel-Kramers-Brillouin method, the quantum numbers (m,n) can be linked to the periodic orbits (p,q) with the equation $k_{m,n}a\sin(p\pi/q) = [m(p/q) + n + (3/4)]\pi$, where m is the azimuthal quantum number, n is the radial quantum number, and $k_{m,n}$ is the eigenvalues [45]. From the correspondence of the orbital angular momentum, another quantum-classical connection can be obtained as $k_{m,n}r_{\min}(p,q) = m$, where $r_{\min}(p,q) = a\cos(p\pi/q)$ is the shortest distance to the circular center for the periodic orbits (p,q) [45]. As a result, the relationship between the average values $(\bar{m},\bar{n})$ and the indices (p,q) can be obtained to determine the parameter u from $\bar{n}/\bar{m} = u/(1-u)$. Figure 7 shows two calculated results for $|G(\mathbf{r},\mathbf{r}';k,\gamma)|$ and $|g(\mathbf{r},\mathbf{r}';k,\gamma,u)|$ of the circular billiard with $\gamma = 0.5\pi/a$ and the source position at $\tilde{x}' = r_{\min}(p,q)$ and $\tilde{y}' = 0$, where $(\bar{m},\bar{n}) = (60,7)$ for the case of $(p,q) = (1,3)$ and $(\bar{m},\bar{n}) = (60,34)$ for the case of $(p,q) = (2,5)$. It can be seen that the spatial distributions $|G(\mathbf{r},\mathbf{r}';k,\gamma)|$ generally display the circular ring patterns, whereas the spatial distributions $|g(\mathbf{r},\mathbf{r}';k,\gamma,u)|$ clearly reveal the patterns related to the classical periodic orbits.

V. SUMMARY

Using the representation of the coherent state in 2D isotropic harmonic oscillators, a decomposing formula related to the beta function is developed to manifest the connection between the quantum Green's function and the individual classical periodic orbits for the 2D integrable systems. The 2D commensurate harmonic oscillators and integrable quantum billiards are numerically analyzed to confirm the practicality of the developed formula. It is found that due to the abundant degeneracy, the correspondence principle of the quantum Green's function in 2D commensurate harmonic oscillators predominantly comes from the superposition of degenerate eigenstates. In contrast, the emergence of classical features in 2D square billiards is found to arise from the superposition of

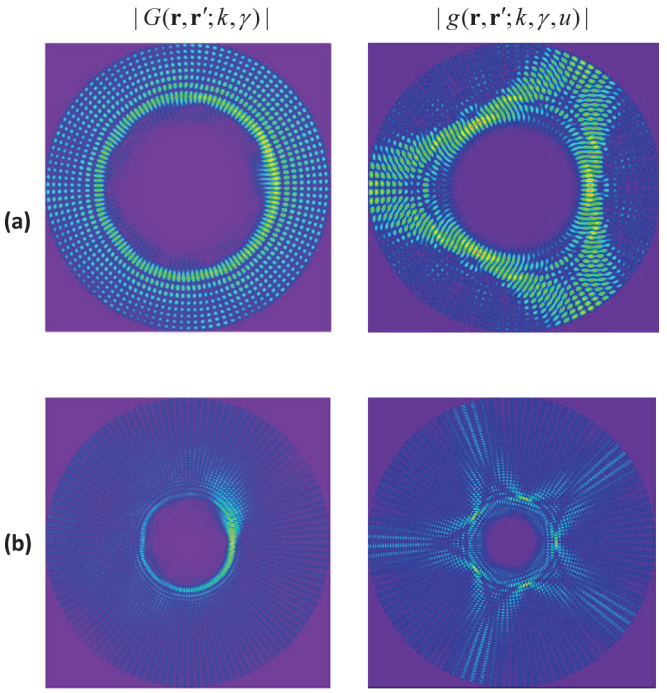

FIG. 7. Calculated results for $|G(\mathbf{r},\mathbf{r}';k,\gamma)|$ and $|g(\mathbf{r},\mathbf{r}';k,\gamma,u)|$ of the circular billiard with $\gamma = 0.5\pi/a$ and the source position at $\tilde{x}' = r_{\min}(p,q)$ and $\tilde{y}' = 0$: (a) $(p,q) = (1,3)$ with $(\bar{m},\bar{n}) = (60,7)$; (b) $(p,q) = (2,5)$ with $(\bar{m},\bar{n}) = (60,34)$.

nearly degenerate eigenstates induced by the tiny damping effect. The present model can provide deep insight into mesoscopic physics [24–27] and transverse pattern formations in laser resonators [31–33,35–39].

ACKNOWLEDGMENT

This work is supported by the Ministry of Science and Technology of Taiwan (Contract No. MOST 105-2628-M-009-004).

[1] L. Challis and F. Sheard, Phys. Today **56**, 41 (2003).
[2] A. Messiah, *Quantum Mechanics* (Wiley, New York, 1966).
[3] S. Mukamel, *Principles of Nonlinear Optical Spectroscopy* (Oxford University Press, New York, 1995).
[4] A. Nitzan, Annu. Rev. Phys. Chem. **52**, 681 (2001).
[5] J. Z. H. Zhang, *Theory and Application of Quantum Molecular Dynamics* (World Scientific, Singapore, 1999).
[6] C. Kittel, *Quantum Theory of Solids* (Wiley, New York, 1963).
[7] J. H. Van Vleck, Proc. Natl. Acad. Sci. USA **14**, 178 (1928).
[8] M. Gutzwiller, J. Math. Phys. **8**, 1979 (1967).
[9] V. M. Strutinsky, A. G. Magner, S. R. Ofengenden and T. Døssing, Z. Phys. A **283**, 269 (1977).
[10] R. Blüumel, *Advanced Quantum Mechanics: The Classical-Quantum Connection* (Jones and Bartlett, Sudbury, MA, 2011).
[11] M. Brack and R. K. Bhaduri, *Semiclassical Physics* (Addison Wesley, Reading, MA, 1997).
[12] M. V. Berry, J. Phys. A **10**, 2083 (1977).
[13] E. J. Heller, Phys. Rev. Lett. **53**, 1515 (1984).
[14] C. Lena, D. Delande, and J. C. Gay, Europhys. Lett. **15**, 697 (1991).
[15] A. J. Makowski and K. J. Górska, J. Phys. A **40**, 11373 (2007).
[16] Y. F. Chen, Phys. Rev. A **83**, 032124 (2011).
[17] J. Xin and J. Q. Liang, Phys. Scr. **90**, 065207 (2015).
[18] A. Bäcker and R. Schubert, J. Phys. A **32**, 4795 (1999).
[19] E. J. Heller, Nature (London) **412**, 33 (2001).
[20] E. J. Heller, Phys. Scr. **T90**, 154 (2001).
[21] A. Bäcker, A. Manze, B. Huckestein, and R. Ketzmerick, Phys. Rev. E **66**, 016211 (2002).
[22] M. Brack, Rev. Mod. Phys. **65**, 677 (1993).
[23] W. A. De Heer, Rev. Mod. Phys. **65**, 611 (1993).
[24] I. V. Zozoulenko and K. F. Berggren, Phys. Rev. B **56**, 6931 (1997).
[25] R. Brunner, R. Meisels, F. Kuchar, R. Akis, D. K. Ferry, and J. P. Bird, Phys. Rev. Lett. **98**, 204101 (2007).
[26] A. D. Peters, C. Jaffé, and J. B. Delos, Phys. Rev. Lett. **73**, 2825 (1994).
[27] C. Bracher and J. B. Delos, Phys. Rev. Lett. **96**, 100404 (2006).
[28] E. Schrödinger, *Collected Papers on Wave Mechanics* (AMS Chelsea Publishing, Providence, RI, 1982).
[29] P. Holland, *The Quantum Theory of Motion* (Cambridge University Press, Cambridge, UK, 1993).
[30] D. Dragoman and M. Dragoman, *Quantum-Classical Analogies* (Springer, Berlin/Heidelberg, 2004).
[31] Y. F. Chen, Y. P. Lan, and K. F. Huang, Phys. Rev. A **68**, 043803 (2003).
[32] Y. F. Chen, T. H. Lu, K. W. Su, and K. F. Huang, Phys. Rev. E **72**, 056210 (2005).
[33] Y. F. Chen, T. H. Lu, K. W. Su, and K. F. Huang, Phys. Rev. Lett. **96**, 213902 (2006).
[34] J. Courtois, A. Mohamed, and D. Romanini, Phys. Rev. A **88**, 043844 (2013).
[35] J. C. Tung, P. H. Tuan, H. C. Liang, K. F. Huang, and Y. F. Chen, Phys. Rev. A **94**, 023811 (2016).
[36] K. F. Huang, Y. F. Chen, H. C. Lai, and Y. P. Lan, Phys. Rev. Lett. **89**, 224102 (2002).
[37] Y. F. Chen, K. F. Huang, and Y. P. Lan, Phys. Rev. E **66**, 046215 (2002).
[38] C. C. Chen, K. W. Su, T. H. Lu, C. C. Liu, Y. F. Chen, and K. F. Huang, Phys. Rev. E **76**, 026219 (2007).
[39] Y. T. Yu, P. H. Tuan, P. Y. Chiang, H. C. Liang, K. F. Huang, and Y. F. Chen, Phys. Rev. E **84**, 056201 (2011).
[40] T. Gensty, K. Becker, I. Fischer, W. Elsäßer, C. Degen, P. Debernardi, and G. P. Bava, Phys. Rev. Lett. **94**, 233901 (2005).
[41] J. D. Louck, M. Moshinsky, and K. B. Wolf, J. Math. Phys. **14**, 692 (1973).
[42] V. Bužek and T. Quang, J. Opt. Soc. Am. B **6**, 2447 (1989).
[43] M. Brack and S. R. Jain, Phys. Rev. A **51**, 3462 (1995).
[44] N. N. Lebedev, *Special Functions & Their Applications* (Dover, New York, 1972).
[45] Y. F. Chen, Y. C. Lin, W. Z. Zhuang, H. C. Liang, K. W. Su, and K. F. Huang, Phys. Rev. A **85**, 043833 (2012).